Geochimica et Cosmochimica Acta Vol. 57, pp. 2585–2597

0016-7037/93/$6.00 + .00

The origin of correlated variations in in-situ $^{18}O/^{16}O$ and elemental concentrations in metamorphic garnet from southeastern Vermont, USA

EDWARD D. YOUNG and DOUGLAS RUMBLE III
Geophysical Laboratory, Carnegie Institution of Washington, Washington, DC 20015-1305, USA

(*Received April* 24, 1992; *accepted in revised form February* 9, 1993)

Abstract—CO_2 laser-heating in a fluorinating atmosphere was used to obtain $^{18}O/^{16}O$ analyses of coexisting garnet, staurolite, muscovite, chlorite, and quartz from a sample of the Gassetts schist, southeastern Vermont, USA. Garnet and quartz $\delta^{18}O_{V\text{-}SMOW}$ values vary on a millimeter scale while values for other minerals are uniform within analytical uncertainties. Garnets exhibit $^{18}O/^{16}O$ zoning with core $\delta^{18}O$ values of 10.9 ± 0.3‰ and rim values of 10.1 ± 0.2. The depletion of ^{18}O in garnet rims correlates with reversals in cation zonation and intracrystalline textural unconformities. Quartz plucked from a garnet core yields a $\delta^{18}O$ of 14.8‰ while vein quartz $\delta^{18}O$ values vary from 14.3 ± 0.2 in centers to 13.8 ± 0.1 at margins. Staurolite, muscovite, and chlorite have mean $\delta^{18}O$ values of 10.8, 11.9, and 10.3, respectively.

Two parageneses are distinguished on the basis of the mineral $\delta^{18}O$ and expected isotope partitioning and on the basis of textures. One consists of garnet cores, staurolite, muscovite, and quartz included in garnet. Garnet rims, chlorite, and vein quartz comprise the other. Quantitative models which explain the lower bulk $\delta^{18}O$ of the garnet-rim assemblage show that garnet textural unconformities represent resorption during infiltration of externally derived aqueous fluid. Chlorite grew by this hydration reaction and was the principal storage site for low $^{18}O/^{16}O$ oxygen. Low-$\delta^{18}O$ garnet rims later grew at the expense of chlorite with little change in modal abundances of staurolite and muscovite. Retention of pre-infiltration $\delta^{18}O$ in muscovite precludes significant diffusion of oxygen in this phase and indicates that the total duration of external fluid flow was $\leq 10^5$ years.

INTRODUCTION

OXYGEN COMPRISES ROUGHLY half of Earth's crust by weight. Exchange of oxygen among crustal phases must therefore reflect the major processes by which matter and energy are transferred during evolution of the tectonosphere. Oxygen isotope ratios have been used to infer mechanisms of oxygen exchange among minerals and fluids during metamorphism (e.g., RUMBLE and SPEAR, 1983). With a few exceptions, however, indisputable evidence that observed heterogeneities in mineral $^{18}O/^{16}O$ are the result of metamorphism has been lacking. RUMBLE et al. (1991a) found that $^{18}O/^{16}O$ values for marbles from southern Maine, USA, are consistent with both extensive fluid-rock interaction during metamorphism and premetamorphic diagenesis. MORRISON and VALLEY (1988) concluded that ^{18}O enrichments in the Marcy Anorthosite Massif of the Adirondack Mountains, USA, are likely to be premetamorphic, magmatic features while TAYLOR (1969) attributed the same enrichments to fluid circulation synchronous with regional metamorphism.

Development of techniques permitting measurement of intracrystalline $^{18}O/^{16}O$ variations in minerals has helped to resolve such ambiguities. By documenting the existence of oxygen isotope zoning in patently metamorphic garnet from southeastern Vermont, USA, CHAMBERLAIN and CONRAD (1991) showed unequivocally that externally derived fluid was present during regional metamorphism. VALLEY and GRAHAM (1991) demonstrated that depletions in ^{18}O within rims of magnetite grains from a marble from the Adirondack Mountains are best explained by exchange with fluid during the waning stages of granulite-grade metamorphism at temperatures well below the maximum.

The utility of intracrystalline heterogeneities in mineral $^{18}O/^{16}O$ can be extended to include the analysis of mineral parageneses in instances where they can be shown to be the result of metamorphism. Inexorable links between chemical concentrations and $^{18}O/^{16}O$ in minerals participating in reactions in which mineral proportions change during metamorphism can be demonstrated mathematically (CHAMBERLAIN et al., 1990; YOUNG, 1991). Natural examples of such expected correlations would constitute clear evidence for contemporaneity of metamorphic reaction and shifts in $^{18}O/^{16}O$. Examples have, to date, not been documented in metamorphic rocks, in part because the spatial resolution of analytical techniques used to measure isotope ratios and those used for determining elemental concentrations differed by orders of magnitude. Emergence of laser-heating fluorination methods for extracting oxygen from silicate and oxide minerals for isotopic analysis (SHARP, 1990) has significantly reduced this disparity in spatial resolution, permitting precise measurement of $^{18}O/^{16}O$ on a millimeter scale.

In this paper, we present an example of the usefulness of millimeter-scale analyses of $^{18}O/^{16}O$ for elucidating the net-transfer reaction history of a pelitic schist. In particular, we present and interpret laser-fluorination $^{18}O/^{16}O$ analyses of metamorphic garnet, staurolite, muscovite, chlorite, and quartz from a Late Proterozoic-Early Cambrian pelitic schist from southeastern Vermont. The sample examined is representative of a class of similar well-studied rocks exposed throughout the region (ROSENFELD, 1968; THOMPSON et al., 1977; KARABINOS, 1984; CHRISTENSEN et al., 1989) and was chosen because a previous study by CHAMBERLAIN and CONRAD (1991) showed that a garnet from a broadly correlative rock is zoned with respect to $^{18}O/^{16}O$. Results

demonstrate that marked discontinuities in cation concentrations and textures in the garnets are attended by changes in $\delta^{18}O$ values and resulted from an episode of garnet resorption involving significant flux of externally derived aqueous fluid.

EXPERIMENTAL METHODS

Oxygen Isotopes

Oxygen was extracted by heating with a 20-watt CO_2 laser in an atmosphere of either BrF_5 or F_2 using a modification of the system described by SHARP (1990). Pressure throughout the extraction was monitored with a capacitance manometer mounted adjacent to the sample chamber. Typical fluorinating agent pressures were between 26 and 133 millibars. Bromine pentafluoride was expanded to the sample chamber following cryogenic distillation. Fluorine gas was delivered by heating $K_2NiF_6 \cdot KF$ powder from 290 to 320°C as described by ASPREY (1976) and RUMBLE et al. (1991b) followed by expansion of evolved F_2 to the sample chamber through a liquid N_2 cold trap. Disposal of excess F_2 was accomplished by reaction with heated KBr.

Whole-grain analyses were performed with a laser power of 5 to 6 W and 0.1 kHz beam modulation. Samples for in-situ analyses consisted of 500 to 300 μm-thick doubly polished circular rock sections 2.5 cm in diameter. In-situ analyses were performed by firing multiple 0.2 to 1.0 second pulses of the unmodulated 5 W laser beam into the sections until the bottom side of the section was completely breached. The O_2-liberating reactions are mediated in all cases by formation of a fluoride melt phase.

Laser irradiance proved to be the most important factor governing the outcome of measurements performed in situ. Laser-beam diameters near the minimum (ca. 100 μm) produced gases with fractionated $\delta^{18}O$ values. Accurate results were obtained when the incident irradiance was decreased by defocusing the beam. Conversely, lowering the irradiance too far to the point where ablation rather than melting occurs during fluorination also results in fractionation. Holes yielding $\delta^{18}O$ values in agreement with whole-grain analyses are approximately 800 μm in diameter. The annular melt zones measure approximately 100 μm in width. Elemental composition maps made with a JEOL JXA-8900L electron microprobe confirm that significantly larger fractions of oxygen remain in melted zones surrounding smaller laser holes compared with those surrounding larger holes.

Extracted oxygen was converted to CO_2 by reaction with a resistance-heated graphite rod in the presence of platinum. Isotope ratios were measured on a Finnigan MAT 252 gas-ratio mass spectrometer. Values are reported in standard per mil deviations (δ) from V-SMOW (Vienna Standard Mean Ocean Water).

Accuracy and precision of the whole-grain laser-fluorination analyses is suggested by duplicate analyses of the McMaster University Oliver Quarry quartz standard (OQQ). The OQQ standard was chosen for routine analysis because of its homogeneity. Typical aliquot sizes of the 120 to 180 mesh OQQ quartz grains ranged from 0.5 to 2.0 mg. The mean $\delta^{18}O_{V\text{-}SMOW}$ obtained over a period of 6 months is 9.8 ± 0.2 (1σ)‰ (Fig. 1). The nominal $\delta^{18}O_{V\text{-}SMOW}$ is 9.9 ± 0.2 as determined by three separate laboratories (SHIEH and SCHWARCZ, 1974). Duplicate conventional analyses of OQQ by one of us (EDY) at Purdue University (1991, unpubl. data) gave 10.0 ± 0.2 concurrent with multiple analyses of NBS-28 averaging 9.7 ± 0.2.

The precision of in-situ analyses of garnet, staurolite, and quartz is no worse than ±0.2‰ judging from reproducibility of analyses of adjacent spots (e.g., data presented). Accuracy of the in-situ analyses is estimated to be near ±0.3‰ or better based on comparisons with whole-grain analyses. For example, four laser-fluorination analyses of chips of staurolite (NH-EY-001) collected from the Littleton Formation of western New Hampshire, USA, yielded a mean $\delta^{18}O_{V\text{-}SMOW}$ of 10.5 ± 0.2 (1σ)‰ in our laboratory with manometrically measured yields of 100% to 103%. Nine in-situ analyses of the NH-EY-001 staurolite show a systematic variation from 9.6 at the rim to 11.0 at the core. The mean of the in-situ analyses is 10.2 ± 0.6 (1σ) where the relatively high standard deviation reflects the core-to-rim zonation. Interlaboratory comparison was afforded by the laboratory at Royal Holloway and Bedford New College, University of London, UK, where a mean of 10.7 ± 0.1 for chips from the same crystal of NH-EY-001 staurolite was obtained (D. Mattey, pers. commun.).

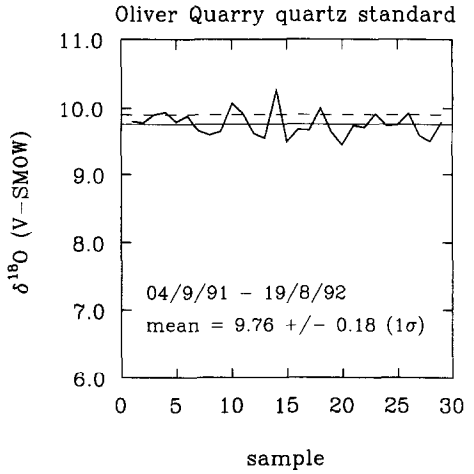

FIG. 1. Summary of whole-grain CO_2 laser-heating fluorination $\delta^{18}O$ analyses of the OQQ quartz standard obtained at the Geophysical Laboratory. Sample sizes for these data ranged from 0.5 to 4.0 mg with oxygen yields averaging 96%. The relatively high scatter of data between samples 10 and 20 derives from problems in focusing the laser which were later corrected. Dashed line shows expected value. Solid line shows the mean value for these data.

Electron Microprobe

Electron microprobe analyses of garnet were performed on the automated wave-length dispersive MAC microprobe housed at the Geophysical Laboratory. Operating conditions included a 15 kV accelerating voltage, 20 nA beam current, 15 micron spot size, and 30 sec counting times (or 30000 counts). Matrix corrections were obtained using the correction factors and methods of BENCE and ALBEE (1968) and ALBEE and RAY (1970). Standards consisted of natural minerals and synthetic glasses. Precision of reported elements is estimated to be ±1%.

SAMPLE DESCRIPTION

The hand sample used in this study (VT-91-13) was collected from an outcrop of the Gassetts schist, a member of the Late Proterozoic-Early Cambrian Hoosac Formation (Fig. 2). Final development of metamorphic assemblages in these rocks is thought to have occurred during the Acadian orogeny (ca. 380 Ma, CHRISTENSEN et al., 1989). Major rock-forming minerals include quartz (Qtz) + white mica (Ms) + chlorite (Chl) + garnet (Grt) + staurolite (St) + biotite (Bt) + graphite (Gr) + ilmenite (Ilm). The rock is characterized macroscopically by nearly monomineralic layers of Qtz and St intercalated with Grt + St + Ms + Chl ± Bt schistose layers.

GARNET ZONING

Description

Garnets are characterized by cores rich in aligned inclusions of chloritoid (Cld), Ms, and Ilm surrounded by asymmetrically distributed rims containing sparse inclusions of Chl and Qtz and embayments containing abundant Qtz and Chl. Relic foliations defined by inclusions in the cores terminate abruptly at core-rim boundaries (Fig. 3). The boundaries can therefore be described as textural unconformities. Detailed petrographic descriptions of analogous garnets from correlative rocks in the region were given by THOMPSON et al. (1977) and KARABINOS (1984).

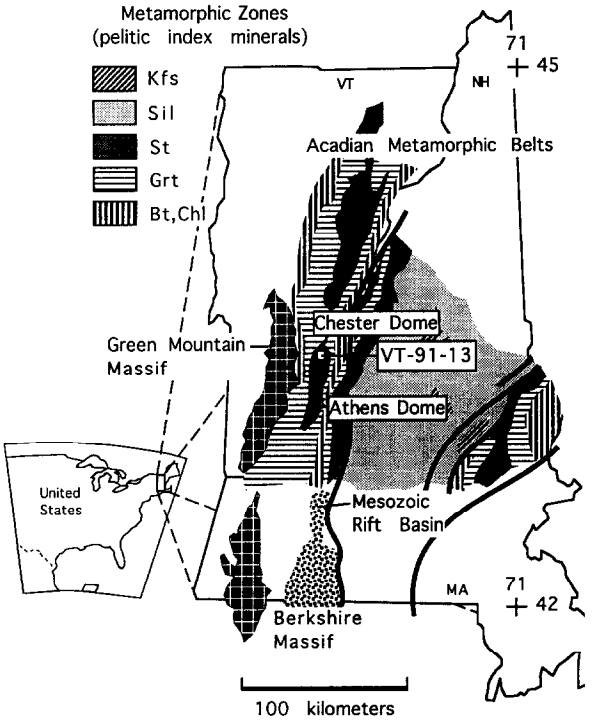

FIG. 2. Simplified map of Acadian metamorphic zones in central and southern Vermont and New Hampshire showing the location of Gassetts schist sample VT-91-13 described in the text. Metamorphic zones (patterns) are delineated on the basis of pelitic index minerals. Mineral abbreviations are those of KRETZ (1983). Bold solid lines are traces of postmetamorphic faults. Thin solid lines are geographic boundaries. Also shown are the Grenville massifs which delimit the western boundary of the Acadian metamorphic belts (black with white grid pattern) and the positions of the Chester and Athens domes (black). Exposures of Gassetts schist and similar rocks are found within the latter structures. Data from ARMSTRONG et al. (1992), CHAMBERLAIN and RUMBLE (1988), and THOMPSON and NORTON (1968).

Transections composed of between twenty and sixty single-spot electron microprobe analyses were obtained for three garnets from sample VT-91-13. Data for two typical traverses are shown in Fig. 4. In every traverse, the textural unconformity in the garnet is coincident with changes in cation concentrations marked by a characteristic peak in Mn (expressed as the mole fraction of spessartine, X_{Sps}, in Fig. 4). Chief among the changes at this X_{Sps} anomaly is the shift from relatively constant and low Mg concentrations (expressed as mole fractions of pyrope, X_{Pyp}) to increasing X_{Pyp} toward the outer edge of the garnet. KARABINOS (1984) described analogous Mn anomalies as marking a reversal from "normal" elemental zoning to "reverse" zoning.

Previous Work

Two prevailing hypotheses have been put forth to explain the unconformities characteristic of garnets from the high-alumina schists belonging to the Hoosac Formation. The features of these proposed reaction histories are summarized succinctly with the aid of two reaction-space polyhedra (Figs. 5 and 6).

Reaction-space polyhedra are geometric constructions which permit portrayal of a rock's reaction history by illustrating the progressive changes in amounts of phases produced or consumed by reaction. The polyhedra are constructed with reference to a reaction space (THOMPSON, 1982; THOMPSON, 1991) defined by orthogonal axes which mark the progress of a subset of linearly independent net-transfer reactions (reactions which involve changes in rock mode). All other net-transfer reactions possible in the system of interest can be described by linear combinations of this subset. In the language of linear algebra, the reactions corresponding to the axes serve as basis vectors which span a reaction space. All other net-transfer reactions are vectors in the reaction space. Progress of any net-transfer reaction is limited by exhaustion of a reactant phase. The locus of points delimiting complete consumption of a phase by reaction is represented by a line (two-dimensional space), a plane (three-dimensional space), or a hyperplane (>3 dimensions) in reaction space. In combination, these features delimit a closed form, or reaction polyhedron (see THOMPSON, 1982). Changes in mode resulting from metamorphic reactions are represented by a sequence of points or paths in a reaction polyhedron.

THOMPSON et al. (1977) concluded that a large garnet from the Gassetts schist recorded a reaction history controlled by a single diastrophic episode. This hypothesis holds that significant portions of the garnet core grew together with staurolite and chlorite by a reaction involving consumption of chloritoid, as illustrated in the reaction polyhedron in Fig. 5. Following consumption of chloritoid, staurolite and biotite grew at the expense of garnet and chlorite, as shown in a separate reaction polyhedron in Fig. 6. Resorption of garnet by this reaction is thought to be represented by the garnet textural unconformities. Garnet rims, in this scenario, represent regrowth at the expense of staurolite, biotite, and possibly chlorite (Fig. 6).

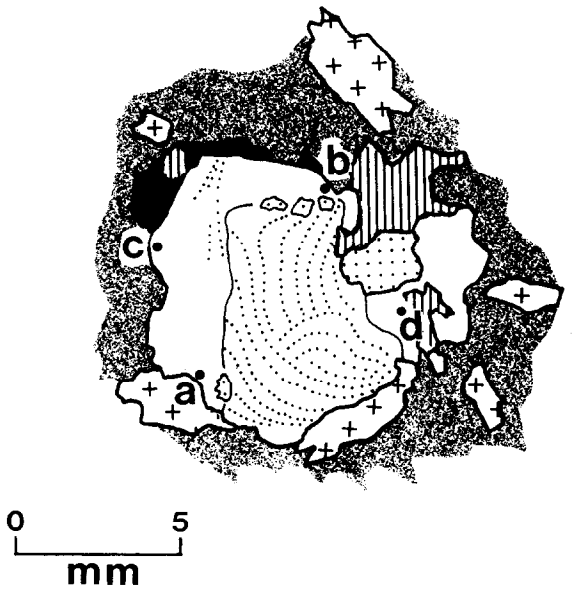

FIG. 3. Map of garnet from sample VT-91-13 showing location of electron microprobe traverses (letters). Symbols: white = Grt; vertical hatch = Chl; black = Bt; crosses = St; stippling = Qtz; mottling = matrix Ms; dotted lines = traces of inclusion trails in garnets; thin solid line = textural unconformity in garnet. Mineral abbreviations after KRETZ (1983).

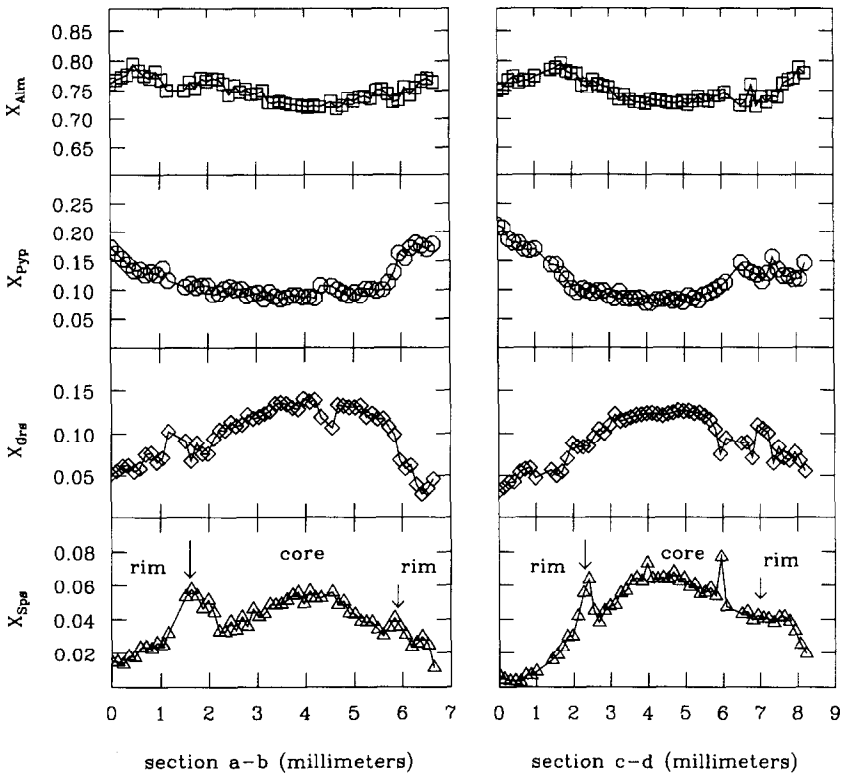

FIG. 4. Electron microprobe analyses of the garnet shown in Fig. 3 along sections a–b and c–d (see Fig. 3) expressed as mole fractions of endmember components. Note abrupt increases in X_{Sps} and X_{Grs} and the change in X_{Pyp} trend associated with the textural unconformity (arrows).

KARABINOS (1985) found that textural unconformities in garnets similar to that studied by THOMPSON et al. (1977) were best explained by growth in response to two distinct diastrophic events (see also ROSENFELD, 1968). In this hypothesis, garnet cores grew principally at the expense of chlorite and chloritoid (Fig. 5). KARABINOS (1985) suggested that garnet resorption was the result of the core-producing reaction operating essentially in reverse. Garnet rims were attributed to a subsequent reaction involving simultaneous growth of garnet and staurolite at the expense of chloritoid and chlorite (Fig. 5).

The importance of the distinction between the two hypotheses described above is underscored by their different geological implications. In the THOMPSON et al. (1977) model, the unconformities in garnets represent a retrograde (on the basis of qualitative arguments, Thompson et al. attributed the resorption to a prograde reaction, but quantitative calculations presented here suggest that their favored resorption reaction is one driven by decreasing temperature) dehydration reaction whereas the model of KARABINOS (1985) implies that the unconformities represent infiltration of aqueous fluid during decreasing temperature and pressure (Fig. 5).

Relation of Oxygen Isotope Data to Previous Work

Suggestions as to the origin of textural unconformities in garnets can be tested using oxygen isotopes. As one example of such a test, consider that an essential feature of the THOMPSON et al. (1977) model is simultaneous growth of garnet cores and staurolite (Fig. 5). If this scenario is correct we should find identical $\delta^{18}O$ values for garnet and staurolite within analytical uncertainties (the equilibrium oxygen isotopic fractionation between garnet and staurolite at temperatures appropriate for these rocks corresponds to a difference in their $\delta^{18}O$ values of less than 0.2‰; e.g., RICHTER and HOERNES, 1988). Present-day $\delta^{18}O$ values for garnet and staurolite can be used with confidence for this test because interiors of these phases are virtually impervious to post-growth $^{18}O^{16}O_{-1}$ exchange. This resistance to oxygen isotopic alteration stems from the slow rates of oxygen self-diffusion in these phases (e.g., FORTIER and GILETTI, 1989). Additionally, since the THOMPSON et al. (1977) model does not involve incorporation of fluid during reaction (Figs. 5 and 6), and because shifts in $\delta^{18}O$ attending advancement of net-transfer reactions in the absence of an externally derived (disequilibrium) fluid are no greater than approximately 0.3‰ (see the following calculations), there is no clear mechanism for affecting significant variations in garnet and staurolite $\delta^{18}O$ during reaction. Uniformity in the oxygen isotopic composition of garnet and staurolite is therefore also expected. Conversely, the model proposed by KARABINOS (1985) suggests that staurolite should be in isotopic equilibrium with garnet rims rather than garnet cores (Fig. 5). Moreover, there is the potential for large shifts in $\delta^{18}O$ values during garnet resorption in the latter model because the resorption reaction is associated with uptake of aqueous fluid. Substantial progress of this reaction would soon deplete pores of their fluid in the rock system, requiring addition of externally derived fluid for continued reaction (Fig. 5). If sufficient amounts of such

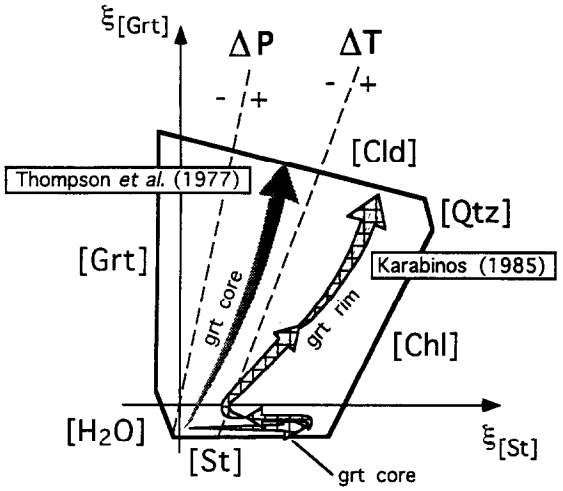

FIG. 5. Modification of the reaction polyhedron used by KARABINOS (1985) to portray his postulate for the net-transfer reaction history and formation of garnet unconformities in the Hoosac Formation, southern Vermont (hatched arrows). Also shown is the garnet-core portion of the reaction history for similar rocks proposed by THOMPSON et al. (1977; grey arrow). Isopleths (dashed) which delimit paths of reactions occurring at constant temperature (ΔT, + and − indicate directions of increasing and decreasing T, respectively) and pressure (ΔP) were calculated for the system CaO-FeO-MgO-MnO-Al_2O_3-SiO_2-H_2O using differential thermodynamics and thermochemical data from SPEAR and CHENEY (1989) and KERRICK and JACOBS (1981). Reaction space axes correspond to forward progress of the reactions Cld + Chl + Qtz = 2Grt + 5H_2O ($\xi_{[St]}$) and 41Cld + 6Qtz = 5Chl + 4St + 17H_2O ($\xi_{[Grt]}$). Precise distances of bounding planes along axes, corresponding to complete consumption of the phase indicated in brackets, will depend upon bulk composition and are shown schematically. Mineral abbreviations are after KRETZ (1983).

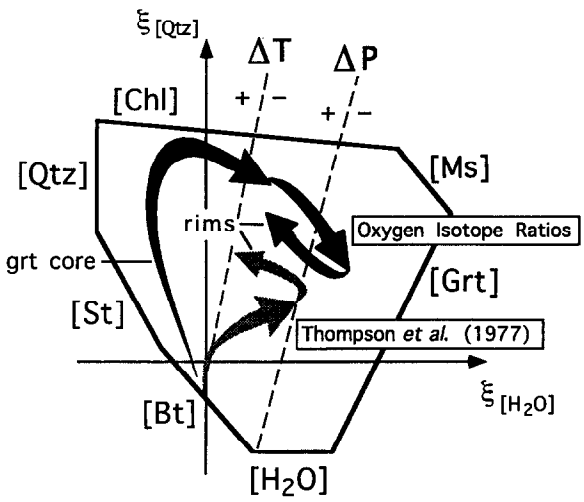

FIG. 6. Reaction polyhedron illustrating the post-garnet core reaction history proposed by THOMPSON et al. (1977) for a sample of the Gassetts schist (grey arrows). Also shown is the reaction history for sample VT-91-13 of the Gassetts schist constrained by the laser-fluorination $\delta^{18}O$ data of the present study (black arrows). Both models indicate that unconformities in garnet are the result of garnet resorption, but the resorption reactions are orthogonal to one another in net-transfer reaction space. Reaction space axes correspond to forward progress of the reactions 47Ms + 3Chl + 58Grt = 12St + 47Bt + 87H_2O (ξ_{H_2O}) and 38Ms + 45Chl = 6St + 29Grt + 38Bt + 174H_2O (ξ_{Qtz}). *P-T* isopleths calculated as for Fig. 4 with the exception that the system includes the component K_2O.

a fluid passed through the rock during reaction, and if the fluid $\delta^{18}O$ values were different from the rock-controlled value, then garnet rims and staurolite could exhibit $\delta^{18}O$ values significantly different from those of garnet cores.

ISOTOPE RESULTS

A thick section of the garnet and its environs shown in Fig. 3 was cut for in-situ analysis of oxygen isotope ratios. A map of the thick section is shown in Fig. 7. The surfaces shown in Figs. 3 and 7 are separated by the material lost during polishing. Consequently, the section used for isotopic analysis lies closer to the center of the garnet than the microprobe section. For comparison with in-situ analyses, additional laser-fluorination data were obtained for small grains (typical sample weights of 0.5 to 1.5 mg) of garnets and associated minerals removed from sample VT-91-13 with the aid of a binocular microscope (Fig. 8). Analysis of whole grains provides nearly 100% oxygen yields and so has the advantage that potential isotopic fractionations associated with incomplete yields necessarily associated with in-situ analyses (see Methods) are eliminated. Results show that mineral $\delta^{18}O$ values vary on a millimeter scale in this sample.

Garnet cores yield $\delta^{18}O_{V\text{-}SMOW}$ values of 10.9 ± 0.3‰ while garnet rims are characterized by $\delta^{18}O_{V\text{-}SMOW}$ values of 10.1 ± 0.1 (Figs. 7 and 8). The map shown in Fig. 7 was made from the thin section of the original thick section used for isotope ratio determinations; the map represents the bottom 30 μm of a 300 μm thick section. As a result, one of the in-situ rim analyses (10.1‰) plots as a core. However, the majority of this sample was obtained from overlying rim material. Quartz ribbons (veins) proximate to the garnets show small systematic variations in $\delta^{18}O$ from values of 14.3

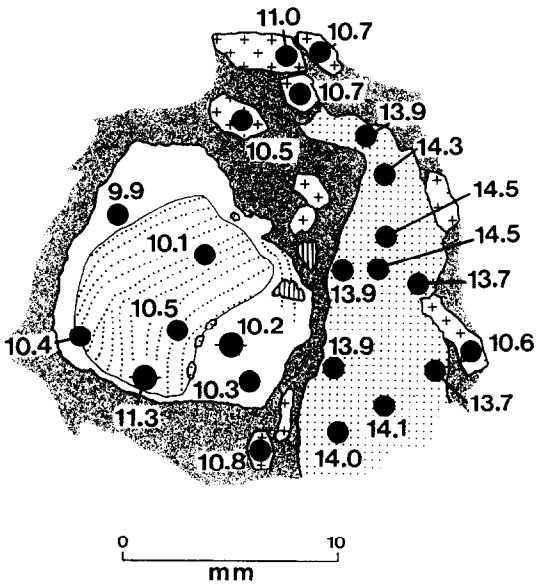

FIG. 7. $\delta^{18}O_{V\text{-}SMOW}$ values for Gassetts schist sample VT-91-13 obtained with in-situ laser-heating fluorination. The analyzed area is a section through the same garnet and environs shown in Fig. 3. Patterned mineral designations are the same as in Fig. 3.

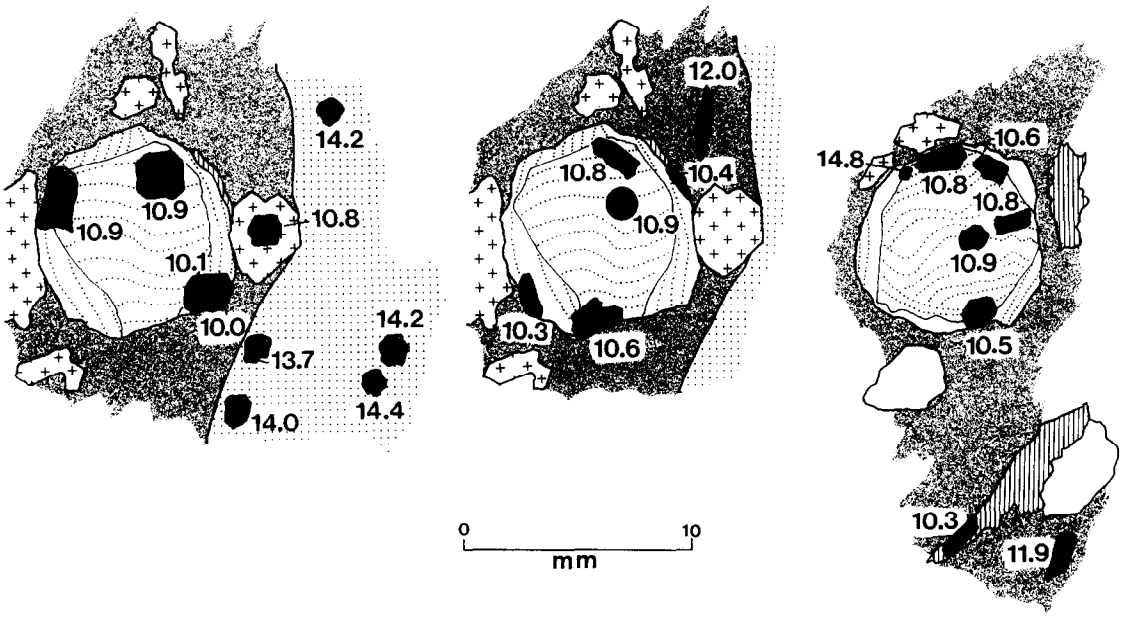

FIG. 8. $\delta^{18}O_{V\text{-}SMOW}$ values for Gassetts schist sample VT-91-13 obtained with laser-heating fluorination of whole grains. Samples are represented by dark grey pattern. Area shown on the left and that shown in the middle are two separate but facing sections of the same garnet and its environs. Patterned mineral designations are the same as in Fig. 3.

± 0.2‰ in vein interiors to 13.8 ± 0.1 along margins (Figs. 7 and 8). A single quartz inclusion plucked from the margin of a garnet core exhibits a higher $\delta^{18}O$ of 14.8‰ (Fig. 8). Staurolite yields uniform $\delta^{18}O$ values of 10.8 ± 0.2. Muscovite and chlorite also show uniform $\delta^{18}O$ values, respectively, within the analytical and spatial resolution of the measurements (Fig. 8).

Two separate parageneses can be distinguished on the basis of the mineral $\delta^{18}O$ data for this sample. The distinction between the assemblages is illustrated using isotope isotherm diagrams (Fig. 9; see JAVOY et al., 1970, for a discussion of isotherm diagrams). The first paragenesis consists of garnet cores, staurolite, muscovite, and the quartz inclusion in garnet. These minerals apparently grew in isotopic equilibrium at a temperature near 590°C (Fig. 9a). Garnet rims, chlorite, and vein quartz comprise the second paragenesis (Fig. 9b). The temperature defined by the garnet rim assemblage is near that of the garnet core assemblage as indicated by the

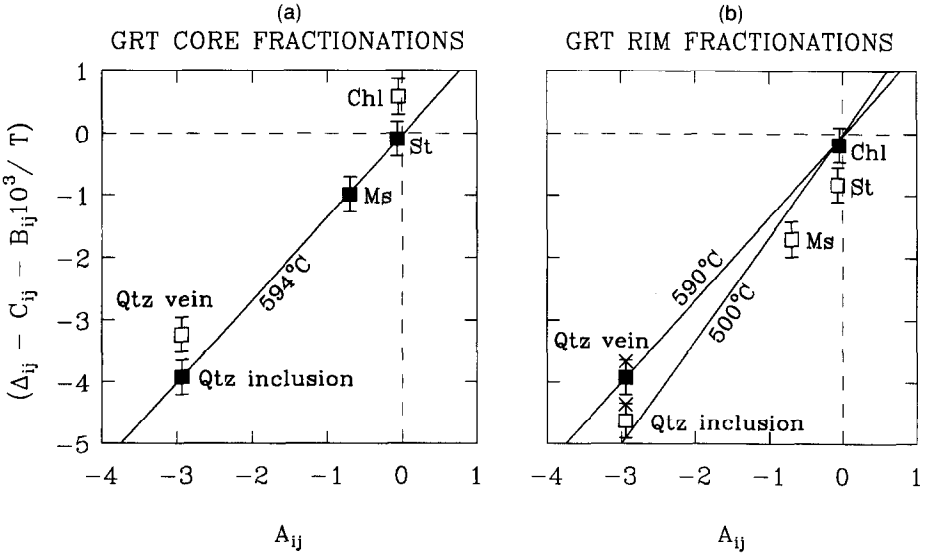

FIG. 9. Oxygen isotope ratio isotherm plots (method of JAVOY et al., 1970) for garnet cores (a) and garnet rims (b) from sample VT-91-13. Each point represents the measured difference between garnet core and rim $\delta^{18}O$ values and the mean values for the indicated mineral (the latter are constant within 1σ of ±0.2‰). Star symbols correspond to extreme $\delta^{18}O$ values found in quartz veins. The two parageneses plot along different but parallel lines (isotherms) owing to a shift in bulk $\delta^{18}O$ composition at nearly constant temperature. The 500°C isotherm (right) is shown for comparison only. Equilibrium fractionation factors are those of RICHTER and HOERNES (1988).

parallel slopes of isotherms (lines passing through the data) in Fig. 9. The two parageneses plot on different (but parallel) isotherms owing to a lowering in bulk $\delta^{18}O$ composition from the older, garnet-core assemblage to the younger, garnet-rim assemblage.

Distinction between the two parageneses suggested by oxygen isotope ratios is supported by textural relations. Garnet cores, staurolite, and muscovite clearly predate garnet rims and chlorite, and garnet rims and chlorite are intergrown (Fig. 3).

ORIGIN OF GARNET ZONING

The origin of the garnet $^{18}O/^{16}O$ zoning is central to the issue of how two parageneses with distinctive oxygen isotope signatures formed in this sample. Four potential causes for isotope zoning in metamorphic garnet are:

1) Progress of a net-transfer reaction in the absence of infiltration of an external fluid.
2) Exchange of oxygen between a ^{18}O-depleted fluid and the interior of the garnets (self-diffusion–controlled exchange).
3) Solution and reprecipitation of garnet in the presence of a ^{18}O-depleted fluid.
4) Progress of a net-transfer reaction in the presence of a ^{18}O-depleted fluid.

Estimates for the rate of oxygen self-diffusion and mass-balance calculations indicate that (1) and (2) are not capable of producing the observed garnet rims. The rims measure several millimeters in width and exhibit $\delta^{18}O$ depletions of ca. 1‰ relative to cores. In contrast, the characteristic length scale of oxygen self-diffusion in garnet at ca. 550°C for a period of 30 Ma is estimated to be only 1×10^{-3} mm (FORTIER and GILETTI, 1989). The self-diffusion of oxygen could not have produced the observed rims in a reasonable time span under normal crustal conditions. Mass-balance calculations (described in detail in the following text) show that the maximum shift in mineral $\delta^{18}O$ resulting from progress of whole-rock net-transfer reactions alone is ≤ 0.3‰ for the Gassetts rocks.

The third potential mechanism for affecting mineral $\delta^{18}O$, dissolution and reprecipitation of garnet in the absence of net-transfer reactions, can result from gradients in chemical potential imposed by differences in surface energy among large and small grains which are otherwise in thermochemical equilibrium (e.g., JOESTEN, 1991; CASHMAN and FERRY, 1988). In principle, this process of grain coarsening, or Ostwald ripening, could explain the $^{18}O/^{16}O$ zoning in garnet if it occurred in the presence of a fluid depleted in ^{18}O relative to the equilibrium fluid composition.

Estimates of the efficacy of grain coarsening were made using the radius-rate relations of JOESTEN (1991). The calculations are based on the premise that the rate of growth or dissolution is controlled by the flux of the slowest diffusing constituent species through the matrix surrounding the garnet porphyroblasts. The matrix is treated as a continuum in which the transport medium is an interconnected fluid occupying the pore space of the rock. Results (Fig. 10) suggest that the rate of coarsening is too slow to account for the size of the low-$\delta^{18}O$ garnet rims, although uncertainties in the input parameters for the calculations (particularly surface energies) preclude definitive rejection of this process as a means for affecting intracrystalline variability in $\delta^{18}O$.

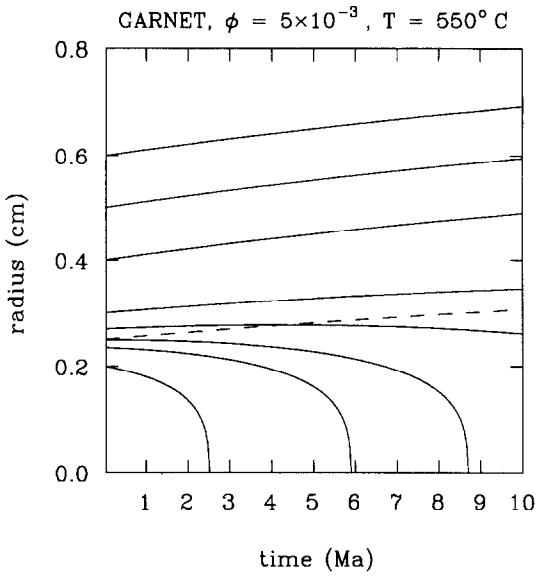

FIG. 10. Radial dissolution-growth curves for garnet porphyroblasts undergoing Ostwald ripening in a continuum matrix with an aqueous fluid-filled porosity of 5.0×10^{-3} at 550°C. Dashed line shows the evolution of the mean radius of the garnet population. Parameters were chosen to be appropriate for modeling the Gassetts schist sample discussed in the text. Calculations were made using the radius-rate relations of JOESTEN (1991), an interfacial energy of 2.0×10^{-4} J/cm^2 suggested by the data of BRACE and WALSH (1962), a rate-limiting cation diffusivity of 2.0×10^{-4} cm^2/sec (OELKERS and HELGESON, 1988), and a solubility appropriate for SiO_2 (one of the most abundant species) given by FOURNIER and POTTER (1982).

Rejection of mechanisms (1) through (3) as implausible leads to the conclusion that net-transfer reaction progress during infiltration of a low $\delta^{18}O$ fluid (the fourth mechanism listed) was the cause of the $^{18}O/^{16}O$ zoning in the garnets. Changes in mineral $\delta^{18}O$ values resulting from reaction and fluid advection operating in parallel can be described by a mass-balance equation for ^{18}O in the interconnected fluid-filled interstices of mineral grains:

$$\frac{\partial C_{^{18}O}^{pore}}{\partial t} = -\text{div}\, J_{^{18}O}^{inf} + \frac{\sigma_{pore}}{v_{pore}} R_{^{18}O}^{nt\text{-}rxn}, \qquad (1)$$

where $C_{^{18}O}^{pore}$ is the concentration of ^{18}O in a fluid-filled pore (an adequate approximation for $^{18}O/^{16}O$ for the purpose at hand), t is time, $J_{^{18}O}^{inf}$ is the advective flux of ^{18}O into the pore attributable to fluid infiltration (mol ^{18}O/cm^2/sec), σ_{pore} is the bounding surface area of the pore, v_{pore} is the volume of the pore, and $R_{^{18}O}^{nt\text{-}rxn}$ is the overall production rate of ^{18}O at pore surfaces (i.e., bounding mineral surfaces) by progress of net-transfer reactions (mol ^{18}O/cm^2/sec). The latter refers to the rate of reaction, irrespective of whether it is controlled by kinetics or changes in ambient conditions which drive the reaction. It is assumed in this formulation that the rates of $^{18}O^{16}O_{-1}$ exchange at mineral surfaces are equal to or greater than the rate of net-transfer reaction (e.g., COLE and OHMOTO, 1986).

Two endmember processes affecting changes in mineral $\delta^{18}O$ are evident from Eqn. 1. One occurs when the net flux of ^{18}O due to fluid flow through the pores ($\mathrm{div}\boldsymbol{J}^{\mathrm{inf}}_{^{18}O}$) keeps pace with the rate of ^{18}O production or consumption by reaction at mineral surfaces ($R^{\mathrm{nt\text{-}rxn}}_{^{18}O}$). In these instances, the concentration of ^{18}O in the pore fluid is constant so that Eqn. 1 reduces to

$$\mathrm{div}\ \boldsymbol{J}^{\mathrm{inf}}_{^{18}O} = \frac{\sigma_{\mathrm{pore}}}{v_{\mathrm{pore}}} R^{\mathrm{nt\text{-}rxn}}_{^{18}O}, \quad (2)$$

and newly grown or exposed mineral surfaces will have $\delta^{18}O$ values which are controlled exclusively by the fluid. This is because the vector portion of Eqn. 1 dominates in this case, and mineral surfaces equilibrate with an infinite reservoir of fluid. Conversely, if the velocity of the fluid cannot keep pace with the rate of reaction we have

$$\mathrm{div}\ \boldsymbol{J}^{\mathrm{inf}}_{^{18}O} \ll \frac{\sigma_{\mathrm{pore}}}{v_{\mathrm{pore}}} R^{\mathrm{nt\text{-}rxn}}_{^{18}O}, \quad (3)$$

such that the new mineral surfaces created during reaction will exhibit $\delta^{18}O$ values reflecting mass balance among minerals and a small integrated volume of pore fluid. The scalar portion of Eqn. 1 dominates in this case, and mineral surfaces equilibrate with a small volume of fluid before they are isolated from further exchange of oxygen by new growth.

Where Eqn. 2 is obtained during mineral growth, the $\delta^{18}O$ values of the minerals which grew during fluid infiltration can be used to compute the oxygen isotopic composition of the fluid directly from equilibrium fractionation factors. However, in instances where condition (3) obtained during growth, a detailed knowledge of the reaction responsible for mineral growth is required if the $^{18}O/^{16}O$ of the fluid is to be ascertained.

ISOTOPE CONSTRAINTS ON REACTION HISTORY

The $\delta^{18}O$ zoning in garnet and the $\delta^{18}O$ values of associated minerals enable reconstruction of the reaction history of this sample of the Gassetts schist. Preservation of staurolite and muscovite $\delta^{18}O$ values reflecting equilibrium with garnet cores (and not rims) requires that the reaction which attended fluid infiltration did not involve significant growth of either mineral (less than approximately 15% by volume for reasonable fluid $\delta^{18}O$). The reaction therefore followed a path roughly parallel to the [Ms] and [St] bounding faces in the reaction polyhedron of Fig. 6. It is evident from Fig. 6 that such reactions involve either growth of garnet or growth of chlorite, but not both at the same time. The peak in Mn concentrations present at the textural unconformity separating the high-$\delta^{18}O$ cores from low-$\delta^{18}O$ rims suggests that the reaction in the case of this sample was one of garnet resorption as Mn is partitioned most strongly to garnet (e.g., SYMMES and FERRY, 1992). Apparently, the oxygen of the infiltrated fluid was incorporated into the rock by growth of chlorite, resulting in the low $\delta^{18}O$ of this mineral in comparison to garnet cores, staurolite, and muscovite. Subsequent regrowth of garnet at the expense of this low-$\delta^{18}O$ chlorite produced the low-$\delta^{18}O$ garnet rims. The qualitative reaction path which is consistent with the $\delta^{18}O$ data is shown in Fig. 6.

Infiltration of aqueous fluid during metamorphism of the schist required by the isotope data is consistent with the suggestion by SYMMES and FERRY (1991) that high fluxes of H_2O-rich fluid are characteristic of regional metamorphism of pelitic rocks. The results of this study are also compatible with the works of FERRY (1992) and STERN et al. (1991) which show that a large deep-seated hydrothermal system existed in the vicinity of the Gassetts schist during Acadian orogenesis.

NUMERICAL SIMULATION OF REACTION HISTORY

Method

Covariations among $^{18}O/^{16}O$ and elemental concentrations in minerals are inevitable consequences of continuous net-transfer reactions in either closed or open systems and are powerful tools for deciphering metamorphic reaction histories. The variations in $\delta^{18}O$ and concentrations of Ca, Fe, Mg, and Mn across garnet unconformities in sample VT-91-13 comprise such a correlation. A numerical model was constructed to investigate whether or not the reaction history summarized qualitatively in Fig. 6 is capable of explaining the observed covariations among garnet $\delta^{18}O$ and cation concentrations. Differential thermodynamics was used for this purpose.

The thermodynamic equations which relate the intensive variables to one another in the formalism of differential thermodynamics are well known (RUMBLE, 1976; SPEAR et al., 1982), as are the methods for numerical integration of the differential equations (SPEAR, 1989). Equations which depict mass-balance and oxygen isotope fractionation can be linked to the intensive-variable equations but are less familiar to many workers.

Extensive variables, including molar quantities of phases M_k and molar amounts of system components η_l^{sys}, are included in thermodynamic calculations by adding to the linear equations relating intensive variables one mass balance equation for each of the independent system components, C in number, of the form (SPEAR, 1988; YOUNG, 1989)

$$0 = \sum_k \left(\sum_j x_{jk}\epsilon_{jkl}\right) dM_k + \sum_k \sum_j (M_k \epsilon_{jkl}) dx_{jk} - d\eta_l^{\mathrm{sys}}, \quad (4)$$

where ϵ_{jkl} is the number of moles of system component l in phase component j, and x_{jk} is the mole fraction of phase component j in phase k. The total variance of the resulting system of equations is $C + 2$, as prescribed by macroscopic thermodynamics (GIBBS, 1948).

Variations in mineral isotope ratios can be included in the thermodynamic analysis described above by addition of equations for the total differentials of $\delta^{18}O$ for each phase i:

$$d\delta^{18}O_i = \left(\frac{\partial \delta^{18}O_i}{\partial T}\right) dT + \sum_k \left(\frac{\partial \delta^{18}O_i}{\partial M_k}\right) dM_k + \sum_f \left(\frac{\partial \delta^{18}O_i}{\partial x_f}\right) dx_f + d\delta^{18}O_{\mathrm{sys}}, \quad (5)$$

where x_f represents the mole-fraction of oxygen-bearing fluid species f in the fluid phase, $d\delta^{18}O_{\mathrm{sys}}$ is the differential of the bulk system $\delta^{18}O$, and T is temperature. The isotope equa-

tions are linked to the thermodynamic and mass-balance equations by the variables dT, dM_k, and in the general case of impure fluid, dx_f. Equation 5 adds one degree of freedom to the system. The increase in variance derives from the distinction between ^{18}O and ^{16}O manifest by the variable $\delta^{18}O_{sys}$. Coefficients for Eqn. 5 are derived by differentiation of the expression

$$\delta^{18}O_i = \sum_s (\omega_s M_s/\tau)\Delta_{is}^T + \sum_f (x_f \omega_f M_{fluid}/\tau)\Delta_{if}^T + \delta^{18}O_{sys}, \quad (6)$$

where ω_s and ω_f are oxygens per mole of solid phase s and fluid species f, respectively; τ is the total number of oxygens in the system; and Δ_{is}^T (Δ_{if}^T) is the temperature-dependent equilibrium difference in $\delta^{18}O$ between phase i and phase s (fluid species f) expressed as

$$\Delta_{is}^T \simeq \frac{A_{is}}{T^2} + \frac{B_{is}}{T} + C_{is}. \quad (7)$$

Equation 6 closely approximates a mass balance equation for ^{18}O (CRAIG, 1953).

For closed systems, $d\eta_1^{sys} = d\eta_2^{sys} = \cdots = d\eta_C^{sys} = d\delta^{18}O_{sys} = 0$, resulting in a total variance of 2 for the complete system of equations. By preserving this total variance, numerical integration of the system of linear differential equations is straightforward (e.g., SPEAR, 1989). In order to model fluid infiltration, therefore, it is desirable to modify the closed-system set of equations to account for variations in η_l^{sys} and $\delta^{18}O_{sys}$ in such a way as to preserve the number of constraints on the resulting equations. One useful approach is to assume negligible porosity changes during fluid infiltration. For the present case, it is sufficient to consider the fluid to be essentially pure H_2O (SYMMES and FERRY, 1991). Defining the system as the rock and its pore volume, the closed-system condition $d\eta_{H_2O}^{sys} = 0$ (constant moles of total system H_2O) is then replaced by $dM_{H_2O} = 0$ (constant moles of the H_2O phase), the tacit assumption being that the fluid occupies dominantly interconnected pores. The total M_{H_2O} at any instant includes both externally derived H_2O and that produced internally by reaction. Note that the number of independent system parameters is not altered by this procedure. Rather, one extensive constraint has simply been replaced by another. Similarly, if the closed-system condition $d\delta^{18}O_{sys} = 0$ can be replaced by an equation relating $\delta^{18}O_{sys}$ to existing parameters of the system, there will be no change in the number of degrees of freedom. The precise form of the equation will depend on the specific circumstance.

A simple example is the case in which $^{18}O/^{16}O$ of the infiltrating H_2O is constant. The equation for $\delta^{18}O_{sys}$ in integrated form is then

$$\delta^{18}O_{sys} = \sum_s \frac{\omega_s M_s}{\tau}\delta^{18}O_s + \frac{M_{H_2O}^{ext}}{\tau}\delta^{18}O_{H_2O}^{ext} + \frac{M_{H_2O}^{int}}{\tau}\delta^{18}O_{H_2O}^{int}, \quad (8)$$

where superscripts ext and int refer to externally derived H_2O and internally produced H_2O, respectively. The oxygen isotopic composition of the internally produced H_2O in Eqn. 8, $\delta^{18}O_{H_2O}^{int}$, is taken to be the value dictated by equilibrium with the solid phases such that only changes in $M_{H_2O}^{ext}$ can affect changes in $\delta^{18}O_{sys}$. Incorporation of the resulting identity

$$dM_{H_2O}^{ext} = d\eta_{H_2O}^{sys}, \quad (9)$$

followed by differentiation of Eqn. 8 yields the new condition for $d\delta^{18}O_{sys}$:

$$d\delta^{18}O_{sys} = \frac{1}{\tau^2}\left(\sum_s \omega_s M_s(\delta^{18}O_{H_2O}^{ext} - \delta^{18}O_s)\right)d\eta_{H_2O}^{sys} + \frac{1}{\tau^2}M_{H_2O}^{int}(\delta^{18}O_{H_2O}^{ext} - \delta^{18}O_{H_2O}^{int})d\eta_{H_2O}^{sys}. \quad (10)$$

Addition of Eqn. 10 to the closed-system equations and replacement of $d\eta_{H_2O}^{sys} = 0$ with $dM_{H_2O} = 0$ produces a set of equations with a total variance of 2, permitting numerical integration by successive evaluations of the associated Jacobian matrix. This was the method used in the present case.

Result

Simulation calculations were performed for an initial bulk composition composed of Qtz (12%) + Ms (33%) + Grt (5%) + Bt (12%) + St (21%) + Chl (12%) ± Pl (4.8%) + H_2O (0.2%) (mineral abbreviations after KRETZ, 1983; abundances in oxygen percent) in the system $K_2^{16}O$-$Na_2^{16}O$-$Ca^{16}O$-$Fe^{16}O$-$Mg^{16}O$-$Mn^{16}O$-$Al_2^{16}O_3$-$Si^{16}O_2$-$H_2^{16}O$-^{18}O. The initial pressure and temperature were taken to be 7000 bar and 590°C, respectively, consistent with estimates for near-peak metamorphism of the Gassetts schist (e.g., KOHN and SPEAR, 1990). Thermochemical data used are given by SPEAR and CHENEY (1989) and YOUNG (1989). Solid activities were defined by mixing-on-sites formulations while the hard-sphere modified Redlich-Kwong equation of state of KERRICK and JACOBS (1981) was used for H_2O. Isotope fractionation factors were taken from RICHTER and HOERNES (1988). Starting $\delta^{18}O$ were calculated from modal abundances, measured $\delta^{18}O$ for garnet-core assemblages (Fig. 9a), and equilibrium isotope fractionation factors. Initial mineral elemental compositions were obtained using a combination of measured garnet, biotite, chlorite, and staurolite compositions and published compositions from similar rocks (e.g., THOMPSON et al., 1977; KARABINOS, 1985).

Reactions in the model Gassetts system are described by four linearly independent net-transfer reactions:

$$55Ms + 63Fe\text{-}Grt + 13\ Mg\text{-}Chl \rightleftharpoons 100Qtz + 55Fe\text{-}Bt + 14Mg\text{-}St + 6Fe\text{-}Chl \quad (r1)$$

$$50Fe\text{-}Bt + 10Mg\text{-}St + 3Fe\text{-}Chl \rightleftharpoons 15Ms + 33Fe\text{-}Grt + 35Al\text{-}Bt + 9Mg\text{-}Chl \quad (r2)$$

$$Ms + Fe\text{-}Grt + Ca\text{-}Grt \rightleftharpoons Fe\text{-}Bt + 3Ca\text{-}Pl \quad (r3)$$

$$27Ms + 6Mg\text{-}Chl + 22Fe\text{-}Chl \rightleftharpoons 6Fe\text{-}Grt + 27Fe\text{-}Bt + 7Mg\text{-}St + 100H_2O \quad (r4)$$

and six exchange reactions (excluding isotopic exchange):

$$MnMg_{-1}[Bt] \rightleftharpoons MnMg_{-1}[Chl] \quad (r5)$$

$$FeMg_{-1}[Bt] \rightleftharpoons FeMg_{-1}[Chl] \quad (r6)$$

$$MnMg_{-1}[St] \rightleftharpoons MnMg_{-1}[Chl] \quad (r7)$$

$$FeMg_{-1}[St] \rightleftharpoons FeMg_{-1}[Chl] \quad (r8)$$

$$MnMg_{-1}[Grt] \rightleftharpoons MnMg_{-1}[Chl] \quad (r9)$$

$$FeMg_{-1}[Grt] \rightleftharpoons FeMg_{-1}[Chl]. \quad (r10)$$

Al-Bt in (r2) is the alumina-rich annite component in Bt, $KFe_2AlAl_2Si_2O_{10}(OH)_2$. Gibbs' phase rule dictates that the system is characterized by three intensive degrees of freedom. The total variance, including both intensive and extensive independent parameters, is 12 ($C + 2$, where C refers to nine oxide system components and ^{18}O) prior to addition of constraints imposed by degree of mobility of components.

For these calculations the system was considered to be closed to transfer of components other than H_2O and ^{18}O, providing the eight extensive constraints $d\eta^{sys}_{i \neq H_2O} = 0$. It was also assumed that externally derived H_2O had a constant $\delta^{18}O$ so that addition of Eqn. 10 constitutes a ninth constraint. Assumption of a constant porosity imparted a tenth restriction, specifically $dM_{H_2O} = 0$. There are then two remaining linearly independent parameters which must be specified in order to calculate the isotopic and thermochemical evolution of the model system.

Since the goal is to examine the system during infiltration of H_2O, one of the two independent parameters was taken as $d\eta^{sys}_{H_2O}$. The value assigned to $d\eta^{sys}_{H_2O}$ is the incremental change in the amount of H_2O used for numerical integration. The magnitude of the increment is somewhat arbitrary, being limited only by the fact that $d\eta^{sys}_{H_2O}$ must be sufficiently small for meaningful numerical integration. The role of Grt is of particular interest, so it proved convenient to choose as the final independent parameter dM_{Grt}. The sign and magnitude assigned to dM_{Grt} relative to $d\eta^{sys}_{H_2O}$ dictates the precise reaction path followed by the rock system. The equations comprising the model Gassetts system were solved by numerical integration using a variety of relative values for dM_{Grt} and $d\eta^{sys}_{H_2O}$.

The low diffusivity of oxygen in both garnet and staurolite precludes isotopic equilibration of the interiors of these phases during reaction. The refractory nature of Grt and St was accounted for in the present calculations by simulating their fractional growth or resorption as a Rayleigh process according to methods described by SPEAR (1988). Invoking fractionation does not significantly alter the results, but is required by preservation of both $\delta^{18}O$ and cation zoning in the garnet.

Results of a simulation which accounts for the covariations in garnet $\delta^{18}O$ and cation concentrations, unconformities in garnet, and $\delta^{18}O$ for coexisting minerals in sample VT-91-13 are shown in Figs. 11 and 12. The model whole-rock reaction during garnet resorption is

$$2.6Grt + 1.3Bt + 0.4St + 7.4H_2O \rightarrow 0.3Qtz + 1.3Ms + 3.0Chl + 0.4Pl. \quad (r11)$$

As suggested by the reaction space analysis (Fig. 6), growth of chlorite at the expense of garnet occurs as a result of de-

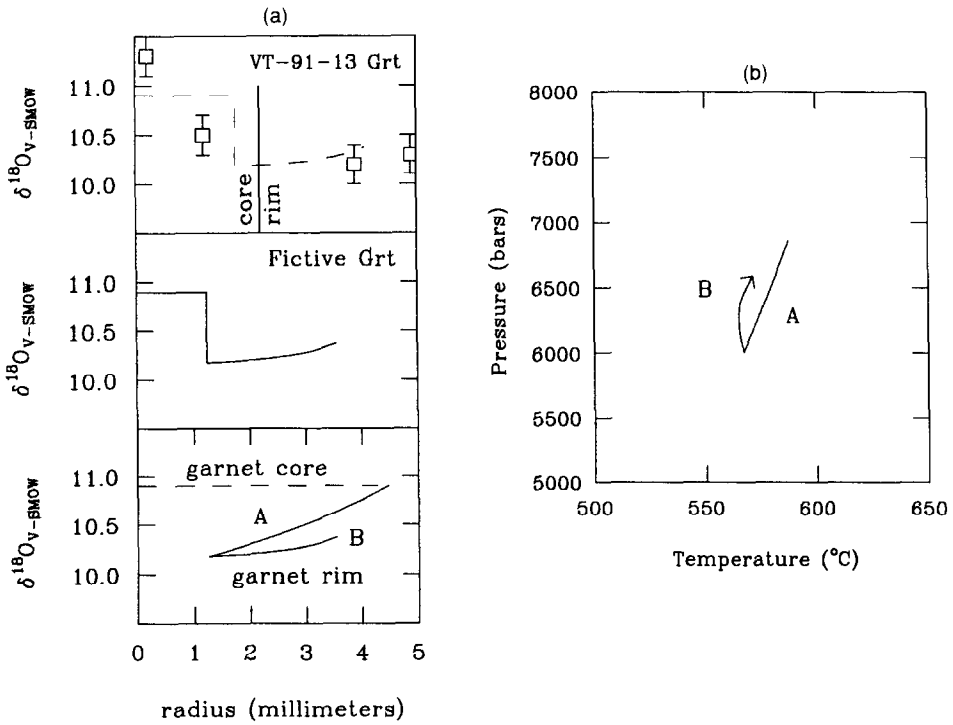

FIG. 11. Results of numerical simulation of the two-stage post-core garnet evolution proposed in the text to explain cation and $\delta^{18}O$ zoning in garnet from Gassetts schist sample VT-91-13. (a) Lower panel shows calculated radius versus $\delta^{18}O_{V\text{-}SMOW}$ for the fictive spherical garnet, middle panel shows the resulting fictive garnet $\delta^{18}O_{V\text{-}SMOW}$ profile, and the upper panel compares the fictive profile with a radial cross-section through the garnet shown in Fig. 7. (b) Pressure-temperature path for the model reaction history in which segments marked "A" and "B" correspond to garnet resorption and regrowth, respectively.

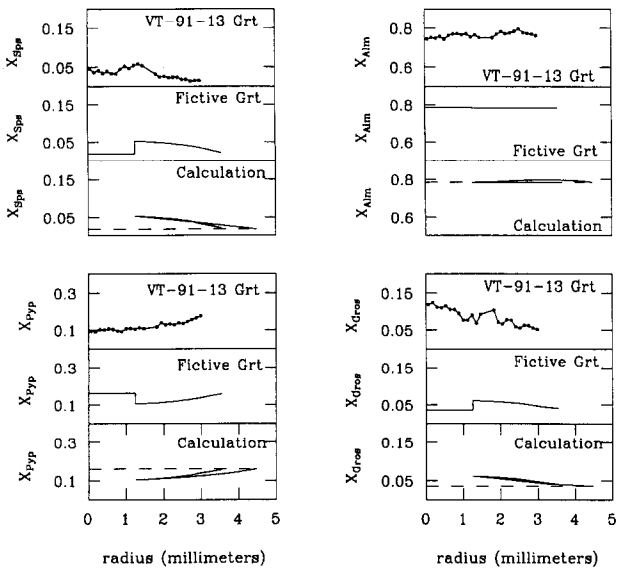

FIG. 12. Comparison between calculated radial profiles for mole fractions of pyrope, spesartine, almandine, and grossular components in fictive spherical garnet derived from the model reaction history shown in Fig. 11 and the observed profiles from the garnet shown in Fig. 3.

creasing temperature and pressure attending addition of H_2O in these calculations.

The isotope data require that no significant changes in bulk $\delta^{18}O$ occurred between growth of chlorite and growth of garnet rims (Fig. 9b). Trial calculations show that garnet growth is accompanied by small changes in $\delta^{18}O$ ($\leq 0.3‰$) in the absence of significant quantities of external aqueous fluid. Consequently, regrowth could have occurred either during infiltration of a fluid similar to (or the same as) that present during chlorite growth or by a dehydration reaction in the absence of fluid flow. Closed-system reaction is precluded by the isotopic evidence against significant participation of hydrous phases other than chlorite (e.g., Fig. 6) and a finite pore volume. We chose to model rim growth as a dehydration reaction. The model reaction for garnet regrowth which is depicted in Figs. 11 and 12 and which reproduces the fundamental features of the garnet rims is

$$2.1\text{Qtz} + 1.2\text{Chl} + 0.3\text{Pl} \rightarrow 2.3\text{Grt} + 0.02\text{St} + 4.6\text{H}_2\text{O}. \quad \text{(r12)}$$

The model regrowth reaction produces negligible changes in garnet $\delta^{18}O$ and reproduces the abrupt increases in Mn and Ca concentrations associated with unconformities, as well as the gradual increase in Mg concentration characteristic of garnet rims. A more precise fit to the garnet composition profiles could be derived by choosing the mole fractions of endmember garnet components as independent variables. This would result in slight variations in the calculated pressure-temperature path shown in Fig. 11 but would not change the salient features of the proposed reaction history.

The precise external fluid $\delta^{18}O$ required to produce the results in Fig. 11 depends upon the relative rates of fluid flow and net-transfer reaction as discussed previously with reference to Eqn. 1. The endmember circumstances described by Eqns. 2 and 3 define the limits for the external fluid $\delta^{18}O$. The limiting case for the rock-dominated environments embodied by Eqn. 3 occurs when each increment of mineral growth occurs in the presence of a single aliquot of pore fluid. The numerical model representing such a process is derived by setting the amount of fluid present in each numerical step equal to the porosity. Results show that a ca. 1‰ lowering of garnet $\delta^{18}O$ (Fig. 11) requires an external fluid $\delta^{18}O$ no greater than approximately 5‰ under these conditions. Alternatively, if the rate of fluid flow was sufficiently great that the steady state described by Eqn. 2 was obtained during mineral growth, the corresponding model would be computed by assigning a quantity of fluid large enough to be numerically infinite at each iteration. As described earlier, the isotope calculations for such fluid-dominated processes are in fact trivial since mineral $\delta^{18}O$ values can be calculated directly from known mineral-fluid fractionations. Equilibrium fractionation between water, chlorite, and garnet suggests that the fluid $\delta^{18}O$ value was 12.0‰ at the temperatures of interest (RICHTER and HOERNES, 1988) if the fluid flux during reaction was sufficient to keep pace with reaction (Eqn. 2). This latter fluid $\delta^{18}O$ is precisely the value indicated by the vein quartz at the same conditions, suggesting that the veins may have been introduced during the same fluid infiltration episode which caused chlorite growth and garnet unconformities. We favor the 12.0‰ value for the fluid and the implied high rate of fluid advection relative to mineral growth because presence of quartz veins is consistent with significant fluid advection (e.g., FERRY, 1992). Additionally, the deep crustal level of metamorphism (KOHN and SPEAR, 1990) would seem to preclude infiltration of meteoric aqueous fluid, and there is no evidence of any other source of fluids which might have the ca. 5‰ oxygen required if fluid velocities were small compared with reaction rates.

DURATION OF FLUID FLOW

An upper limit to the duration of fluid infiltration is indicated by the fact that muscovite has retained $\delta^{18}O$ values approaching equilibrium with garnet cores. The temporal constraints result from knowledge of the rate of oxygen self-diffusion in muscovite (FORTIER and GILETTI, 1991). To illustrate these constraints, the equilibrium $\delta^{18}O$ of 12.0‰ for aqueous fluid indicated by chlorite, garnet rims, and vein quartz was used to compute diffusion profiles of $\delta^{18}O$ in muscovite assuming an infinite cylinder geometry for the grains. The cylinders of mica were considered to be characterized by a homogeneous initial $\delta^{18}O$ value of 11.9‰ ($\delta^{18}O_i$) commensurate with observed values. The homogeneous mica cylinders were then envisioned to be completely surrounded by an infinite reservoir of the low-$\delta^{18}O$ fluid at 550°C. Mica surfaces were held in isotopic equilibrium with the fluid throughout the calculations ($\delta^{18}O_{eq}$). The solution to the diffusion equation for these boundary and initial conditions for a cylinder of maximum radius a is given by CRANK (1956):

$$\frac{\delta^{18}O_r - \delta^{18}O_i}{\delta^{18}O_{eq} - \delta^{18}O_i} = 1 - \frac{2}{a}\sum_{n=1}^{\infty} \frac{\exp(-D\alpha_n^2 t) J_0(r\alpha_n)}{\alpha_n J_1(a\alpha_n)} \quad (11)$$

where $\delta^{18}O_r$ represents values of $\delta^{18}O$ at radius r. $J_0(r\alpha_n)$ and $J_1(a\alpha_n)$ are Bessel functions of the indicated order and α_n denotes roots satisfying

$$J_0(a\alpha_n) = 0. \quad (12)$$

We sampled whole grains of muscovite with the laser. Diffusion profiles were accordingly integrated to yield apparent bulk mica $\delta^{18}O$ values. Integration was accomplished by deriving quadratic fits to the diffusion profiles calculated from Eqn. 11 (correlation coefficients for the fit equations exceed 0.99) of form

$$\delta^{18}O_r = Ar^2 + Br + C. \quad (13)$$

It follows from Eqn. 13 that the expression for bulk mica $\delta^{18}O$ values is

$$\frac{1}{a^2}\int_{r=0}^{r=a} \delta^{18}O_r d(r^2) = \frac{1}{2}Aa^2 + \frac{2}{3}Ba + C. \quad (14)$$

A plot of integrated $\delta^{18}O$ against time and effective radius (Fig. 13) shows that preservation of the muscovite $\delta^{18}O$ required a duration of flow of less than ca. 50,000 years. Longer times would have resulted in diffusive reconstitution of muscovite $\delta^{18}O$ toward values imparted by equilibration with the invaded fluid. The upper limit on the duration of fluid-rock interaction does not allow for episodic flow so the total time represented by growth of chlorite (path A in Fig. 11) may have been greater. Indeed, denudation of approximately 3 km of crust implied by the decompression path which apparently caused chlorite growth (Fig. 11, path A) would be unlikely to be accomplished in less than 10^6 years in view of average rates of tectonic motions. Nevertheless, it is noteworthy that AGUE (1992) has suggested that the duration of fracture-controlled fluid flow through rocks of similar grade from Connecticut was also on the order of 10^4 years or less.

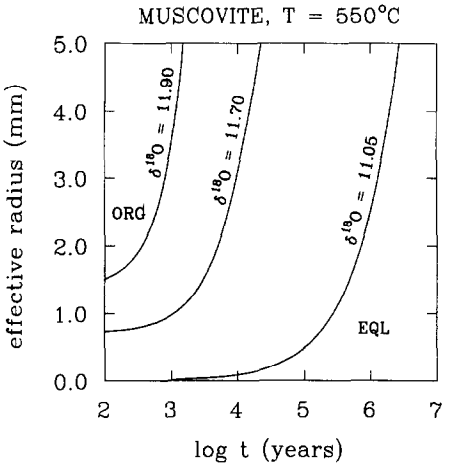

FIG. 13. Plot of effective radius of cylindrical muscovite vs. time illustrating expected shifts in integrated (bulk) muscovite $\delta^{18}O$ as a result of self-diffusion of oxygen. For comparison, typical muscovite grain size in sample VT-91-13 is <2 mm. The muscovite surfaces were assumed to be in isotopic equilibrium with an ambient aqueous fluid with $\delta^{18}O$ of 12.0‰ (dictated by equilibrium with VT-91-13 garnet rims) while the grain interiors were initially set to the value observed in sample VT-91-13. ORG = original $\delta^{18}O_{V\text{-}SMOW}$ of muscovite. EQL = $\delta^{18}O_{V\text{-}SMOW}$ after complete equilibration with fluid. Diffusion coefficients were calculated from data of FORTIER and GILETTI (1991). Infinite-cylinder solution to the diffusion equation for constant surface composition was taken from CRANK (1956).

CONCLUSIONS

Millimeter-scale maps of $^{18}O/^{16}O$ afforded by laser heating in a sample of high-alumina schist from southeastern Vermont, USA, establish that pronounced textural and compositional intracrystalline garnet unconformities are the result of a short-lived fluid infiltration episode in the sample examined.

Identification of $^{18}O/^{16}O$ zoning in garnet and comparisons with $^{18}O/^{16}O$ data for coexisting minerals with varied oxygen transport characteristics permit reconstruction of the modes of oxygen transfer which attended amphibolite-grade metamorphism of the schist sample. Results show that the principal mechanism for oxygen exchange during metamorphism was progress of a continuous net-transfer reaction concurrent with infiltration of aqueous fluid depleted in ^{18}O relative to the schist. The reaction which enabled exchange of oxygen between fluid and rock involved consumption of garnet and growth of chlorite. A maximum limit to the integrated duration of fluid-rock interaction of approximately 10^4 to 10^5 years is provided by the lack of oxygen isotope exchange between fluid and white micas which did not participate in the hydration reaction. Initially, product chlorite served as the principal storage site for the fluid-derived oxygen. Reaction involving garnet regrowth at the expense of the low-^{18}O chlorite caused redistribution of oxygen and resulted in $^{18}O/^{16}O$ zoning in garnets.

Results of this study portend the utility of millimeter-scale maps of $^{18}O/^{16}O$ for identifying reactions which occurred during metamorphism. If further study substantiates the conclusion that garnet unconformities, which are characteristic of high-alumina schists correlative with the sample examined here, are the result of punctuated fluid infiltration, an important and previously unrecognized aspect of the evolution of these rocks will have been identified.

Acknowledgments—We thank G. E. Bebout for supplying us with the sample of Gassetts schist and J. M. Palin for aid in developing laser-fluorination techniques. C. P. Chamberlain and Z. D. Sharp offered many valuable suggestions regarding analytical techniques. Quartz standard OQQ was kindly supplied by Y. N. Shieh. D. George is acknowledged for his help in operating the electron microprobe and scanning electron microscope. We have benefited from the advice of J. M. Brenan and T. C. Hoering throughout this study. The present manuscript represents improvements following constructive reviews by C. P. Chamberlain and an anonymous reviewer.

Editorial handling: G. Faure

REFERENCES

AGUE J. (1992) Hydrochemical differentiation during metamorphism of pelites: Fracture flow-controlled major element mass transfer and the growth of Barrovian zone index minerals. *GSA Abstr. Prog.* **24,** A264 (abstr.).

ALBEE A. L. and RAY L. (1970) Correction factors for electron probe microanalysis of silicates, oxides, carbonates, phosphates, and sulfates. *Anal. Chem.* **42,** 1408–1414.

ARMSTRONG T. R., TRACY R. J., and HAMES W. E. (1992) Contrasting styles of Taconian, Eastern Acadian and Western Acadian metamorphism, central and western New England. *J. Metam. Geol.* **10,** 415–426.

ASPREY L. B. (1976) The preparation of very pure fluorine gas. *J. Fluorine Chem.* **7,** 359–361.

BENCE A. E. and ALBEE A. L. (1968) Empirical correction factors for the electron microanalysis of silicates and oxides. *J. Geol.* **76,** 382–403.

BRACE W. F. and WALSH J. B. (1962) Some direct measurements of the surface energy of quartz and orthoclase. *Amer. Mineral.* **47,** 1111–1122.

CASHMAN K. V. and FERRY J. M. (1988) Crystal size distribution (CSD) in rocks and the kinetics and dynamics of crystallization. *Contrib. Mineral. Petrol.* **99,** 401–415.

CHAMBERLAIN C. P. and CONRAD M. E. (1991) Oxygen isotope zoning in garnet. *Science* **254,** 403–406.

CHAMBERLAIN C. P. and RUMBLE D., III (1988) Thermal anomalies in a regional metamorphic terrane: An isotopic study of the role of fluids. *J. Petrol.* **29,** 1215–1232.

CHAMBERLAIN C. P., FERRY J. M., and RUMBLE D., III (1990) The effect of net-transfer reactions on the isotopic composition of minerals. *Contrib. Mineral. Petrol.* **105,** 322–336.

CHRISTENSEN J. N., ROSENFELD J. L., and DEPAOLO D. J. (1989) Rates of tectonometamorphic processes from rubidium and strontium isotopes in garnet. *Science* **244,** 1465–1469.

COLE R. E. and OHMOTO H. (1986) Kinetics of isotopic exchange at elevated temperatures and pressures. In *Stable Isotopes in High Temperature Geological Processes* (ed. J. W. VALLEY et al.); *Rev. Mineral. 16,* pp. 41–90.

CRAIG H. (1953) The geochemistry of the stable carbon isotopes. *Geochim. Cosmochim. Acta* **3,** 53–92.

CRANK J. (1956) *The Mathematics of Diffusion.* Oxford Univ. Press.

FERRY J. M. (1992) Regional metamorphism of the Waits River Formation, eastern Vermont: Delineation of a new type of giant metamorphic hydrothermal system. *J. Petrol.* **33,** 45–94.

FORTIER S. M. and GILETTI B. J. (1989) An empirical model for predicting diffusion coefficients in silicate minerals. *Science* **245,** 1481–1484.

FORTIER S. M. and GILETTI B. J. (1991) Volume self-diffusion of oxygen in biotite, muscovite, and phlogopite micas. *Geochim. Cosmochim. Acta* **55,** 1319–1330.

FOURNIER R. O. and POTTER I. (1982) An equation correlating the solubility of quartz in water form 25° to 900°C at pressures up to 10,000 bars. *Geochim. Cosmochim. Acta* **46,** 1969–1973.

GIBBS J. W. (1948) On the equilibrium of heterogeneous substances. In *The Collected Works of J. Willard Gibbs,* pp. 55–86. Yale Univ. Press.

JAVOY M., FOURCADE S., and ALLÉGRE C. J. (1970) Graphical method of examination of $^{18}O/^{16}O$ fractionations in silicate rocks. *Earth Planet. Sci. Lett.* **10,** 12–16.

JOESTEN R. L. (1991) Kinetics of coarsening and diffusion-controlled mineral growth. In *Contact Metamorphism* (ed. D. M. KERRICK); *Rev. Mineral. 26,* pp. 507–582.

KARABINOS P. (1984) Polymetamorphic garnet zoning from southeastern Vermont. *Amer. J. Sci.* **284,** 1008–1025.

KARABINOS P. (1985) Garnet and staurolite producing reactions in a chlorite-chloritoid schist. *Contrib. Mineral. Petrol.* **90,** 262–275.

KERRICK D. M. and JACOBS G. K. (1981) A modified Redlich-Kwong equation for H_2O, CO_2, and H_2O-CO_2 mixtures at elevated pressures and temperatures. *Amer. J. Sci.* **281,** 735–767.

KOHN M. J. and SPEAR F. S. (1990) Two new geobarometers for garnet amphibolites, with applications to southeastern Vermont. *Amer. Mineral.* **75,** 89–96.

KRETZ R. (1983) Symbols for rock-forming minerals. *Amer. Mineral.* **68,** 277–279.

MATSUHISA Y., GOLDSMITH J. R., and CLAYTON R. N. (1979) Oxygen isotopic fractionation in the system quartz-albite-anorthite-water. *Geochim. Cosmochim. Acta* **43,** 1131–1140.

MORRISON J. and VALLEY J. W. (1988) Contamination of the Marcy Anorthosite Massif, Adirondack Mountains, NY: Petrologic and isotopic evidence. *Contrib. Mineral. Petrol.* **98,** 97–108.

OELKERS E. H. and HELGESON H. C. (1988) Calculation of the thermodynamic and transport properties of aqueous species at high pressures and temperatures: Aqueous tracer diffusion coefficients of ions to 1000°C and 5 kb. *Geochim. Cosmochim. Acta* **52,** 63–85.

RICHTER R. and HOERNES S. (1988) The application of the increment method in comparison with experimentally derived and calculated O-isotope fractionations. *Chem. Erde* **48,** 1–18.

ROSENFELD J. L. (1968) Garnet rotations due to major Paleozoic deformations in southeastern Vermont. In *Studies in Appalachian Geology—Northern and Maritime* (ed. E. ZEN et al.), pp. 185–202. Interscience.

RUMBLE D., III (1976) The use of mineral solid solutions to measure chemical potential gradients in rocks. *Amer. Mineral.* **61,** 1167–1174.

RUMBLE D., III, and SPEAR F. S. (1983) Oxygen-isotope equilibration and permeability enhancement during regional metamorphism. *J. Geol. Soc. London* **140,** 619–628.

RUMBLE D., III, OLIVER N. H. S., FERRY J. M., and HOERING T. C. (1991a) Carbon and oxygen isotope geochemistry of chlorite-zone rocks of the Waterville limestone, Maine, USA. *Amer. Mineral.* **76,** 857–866.

RUMBLE D., III, PALIN M. J., and HOERING T. C. (1991b) Laser fluorination of sulfide minerals with F_2 gas. *Ann. Rpt. Director Geophys. Lab., Carnegie Inst. Washington, 1990–1991,* 30–34.

SCHÜTZE H. (1980) Der Isotopenindex—Eine Inkrementenmethode zur näherungsweisen Berechnung von Isotopenaustauschgleichgewichten zwischen kristallinen Substanzen. *Chem. Erde* **39,** 321–334.

SHARP Z. D. (1990) A laser-based microanalytical method for the in situ determination of oxygen isotope ratios of silicates and oxides. *Geochim. Cosmochim. Acta* **54,** 1353–1358.

SHIEH Y. N. and SCHWARCZ H. P. (1974) Oxygen isotope studies of granite and migmatite, Grenville province of Ontario, Canada. *Geochim. Cosmochim. Acta* **38,** 21–45.

SPEAR F. S. (1988) The Gibbs method and Duhem's theorem: The quantitative relationship among P, T, chemical potential, phase composition and reaction progress in igneous and metamorphic systems. *Contrib. Mineral. Petrol.* **99,** 249–256.

SPEAR F. S. (1989) Petrologic determination of metamorphic pressure-temperature-time paths. In *Metamorphic Pressure-Temperature-Time Paths* (ed. F. S. SPEAR and S. M. PEACOCK); *Amer. Geophys. Union Short Course 7,* pp. 1–55.

SPEAR F. S. and CHENEY J. T. (1989) A petrogenetic grid for pelitic schists in the system SiO_2-Al_2O_2-FeO-MgO-K_2O-H_2O. *Contrib. Mineral. Petrol.* **101,** 149–164.

SPEAR F. S., FERRY J. M., and RUMBLE D., III (1982) Analytical formulation of phase equilibria: The Gibbs' method. In *Characterization of Metamorphism through Mineral Equilibria* (ed. J. M. FERRY); *Rev. Mineral. 16,* pp. 105–152.

STERN L. A., CHAMBERLAIN C. P., BARNETT D. E., and FERRY J. M. (1991) Stable isotopic evidence for regional-scale fluid migration in a Barrovian metamorphic terrane, Vermont, USA. *GSA Abstr. Prog.* **23,** A335 (abstr.).

SYMMES G. H. and FERRY J. M. (1991) Evidence from mineral assemblages for infiltration of pelitic schists by aqueous fluids during metamorphism. *Contrib. Mineral. Petrol.* **108,** 419–438.

SYMMES G. H. and FERRY J. M. (1992) The effect of whole-rock MnO content on the stability of garnet in pelitic schists during metamorphism. *J. Metam. Petrol.* **10,** 221–237.

TAYLOR H. P. (1969) Oxygen isotope studies of anorthosites, with particular reference to the origin of bodies in the Adirondack Mountains, New York. In *Origin of Anorthosite and Related Rocks* (ed. Y. W. ISACHSEN); *New York State Mus. Sci. Ser. Mem. 18,* pp. 111–134.

THOMPSON J. B., JR. (1982) Reaction space: An algebraic and geometric approach. In *Characterization of Metamorphism through Mineral Equilibria* (ed. J. M. FERRY); *Rev. Mineral. 16,* pp. 33–52.

THOMPSON J. B., JR. (1991) Modal space: Applications to ultramafic and mafic rocks. *Canadian Mineral.* **29,** 615–632.

THOMPSON J. B. and NORTON S. A. (1968) Paleozoic regional metamorphism in New England and adjacent areas. In *Studies in Appalachian Geology—Northern and Maritime* (ed. E. ZEN et al.), pp. 319–327. Interscience. New York.

THOMPSON A. B., TRACY R. J., LYTTLE P. T., and THOMPSON J. B., JR. (1977) Prograde reaction histories deduced from compositional zonation and mineral inclusions in garnet from the Gassetts schist, Vermont. *Amer. J. Sci.* **277,** 1152–1167.

VALLEY J. W. and GRAHAM C. M. (1991) Ion microprobe analysis of oxygen isotope ratios in granulite facies magnetites: Diffusive exchange as a guide to cooling history. *Contrib. Mineral. Petrol.* **109,** 38–52.

YOUNG E. D. (1989) Petrology of biotite-cordierite-garnet gneiss of the McCullough Range, Nevada II. P-T-a_{H_2O} path and growth of cordierite during late stages of low-P granulite-grade metamorphism. *J. Petrol.* **30,** 61–78.

YOUNG E. D. (1991) The relationship between reaction progress and $^{18}O/^{16}O$ in metamorphic minerals: A general analytical approach. *GSA Abstr. Prog.* **23,** A393 (abstr.).